energies

MDPI

Article

Data-Driven Air-Fuel Path Control Design for Robust RCCI Engine Operation

Jan Verhaegh [1], Frank Kupper [1] and Frank Willems [1,2,*]

[1] Powertrains Department, TNO Automotive , 5700 AT Helmond, The Netherlands; jan.verhaegh@tno.nl (J.V.); frank.kupper@tno.nl (F.K.)
[2] Control Systems Technology, Department of Mechanical Engineering, Eindhoven University of Technology, 5600 MB Eindhoven, The Netherlands
* Correspondence: frank.willems@tno.nl

Abstract: Reactivity controlled compression ignition (RCCI) is a highly efficient and clean combustion concept, which enables the use of a wide range of renewable fuels. Consequently, this promising dual fuel combustion concept is of great interest for realizing climate neutral future transport. RCCI is very sensitive for operating conditions and requires advanced control strategies to guarantee stable and safe operation. For real-world RCCI implementation, we face control challenges related to transients and varying ambient conditions. Currently, a multivariable air–fuel path controller that can guarantee robust RCCI engine operation is lacking. In this work, we present a RCCI engine controller, which combines static decoupling and a diagonal MIMO feedback controller. For control design, a frequency domain-based approach is presented, which explicitly deals with cylinder-to-cylinder variations using data-driven, cylinder-individual combustion models. This approach enables a systematic trade-off between fast and robust performance and gives clear design criteria for stable operation. The performance of the developed multivariable engine controller is demonstrated on a six-cylinder diesel-E85 RCCI engine. From experimental results, it is concluded that the RCCI engine controller accurately tracks the five desired combustion and air path parameters, simultaneously. For the studied transient cycle, this results in 12.8% reduction in NO_x emissions and peak in-cylinder pressure rise rates are reduced by 3.8 bar/deg CA. Compared to open-loop control, the stable and safe operating range is increased from 25 °C up to 35 °C intake manifold temperature and maximal load range is increased by 14.7% up to BMEP = 14.8 bar.

Keywords: dual fuel control; combustion modelling; combustion engine system control; data-driven models; model-based control; alternative fuels; fuel flexibility

Citation: Verhaegh, J.; Kupper, F.; Willems, F. Data-Driven Air-Fuel Path Control Design for Robust RCCI Engine Operation. *Energies* **2022**, *15*, 2018. https://doi.org/10.3390/en15062018

Academic Editors: Maria Cristina Cameretti and Gabriele Di Blasio

Received: 20 December 2021
Accepted: 25 February 2022
Published: 10 March 2022

1. Introduction

The transport sector faces enormous challenges in contributing to a climate neutral society in 2050. With the European Green Deal, an ambitious 2050 sector target of 90% green house gas (GHG) reduction, with respect to 1990 emissions, was set [1]. To achieve this long term sustainability goal, intermediate targets were also defined. For new European on-road vehicles, legislation requires that the tailpipe CO_2 emissions (in g/km) are cut by 30% to 40% in 2030 (using a 2019 reference). Moreover, the maritime sector has defined their targets: at least a 40% reduction in carbon intensity of all ships in 2030 compared to the 2008 baseline. At the same time, increasingly strict targets for pollutant emissions have to be met. For on-road applications, attention is shifting towards real-world emissions, particularly nitrogen oxide (NO_x) and particulate matter (PM), to improve local air quality.

Internal combustion engines are the workhorses in the transport sector, especially for heavy-duty applications. Typically, these applications cannot be easily converted into full electric applications. Consequently, it is of major importance to focus on alternative concepts that can be introduced on relatively short time frames, such that they start accelerating the reduction of GHG emissions. From a well-to-wheel system perspective, besides

influencing human behavior and introducing vehicle and logistic measures, highly efficient engine concepts running on renewable fuels is a promising alternative. This not only holds for heavy-duty applications, but also for passenger cars. Using renewable fuels offers an important advantage: the possibility to use existing fuelling infrastructure. Note that the current focus on tailpipe CO_2 emission reduction does not promote the use of renewable fuels. However, this is expected to change by new on-road legislation for the post-2030 time frame. In addition, a recent study into life cycle-related GHG emissions of passenger cars [2] showed that the combination of plug-in hybrid electric vehicles and renewable E85 or HVO is expected to be competitive with battery electric vehicles in 2050.

1.1. Fuel Flexible RCCI Concept

Reactivity controlled compression ignition (RCCI) is an advanced dual-fuel combustion concept that is characterized by very high thermal efficiencies (up to 57%) as well as ultra-low engine-out, NO_x, and PM emissions [3]. In this fuel flexible concept, a low reactivity (gasoline-like) and high reactivity (diesel-like) fuel is blended in the cylinder to create the desired combustion properties. This makes it robust for the selection of future sustainable transport fuels. In this work, we focus on the combination of diesel and E85, which are commercially available and show good combustion properties, see, e.g., [4–6]. Although massive progress has been made in the understanding of the RCCI concept, four main challenges are encountered in competing with alternative concepts, and they bring this promising concept "on the road: [6]:

1. Realizing high brake thermal efficiencies (above 50%);
2. Stable engine operations over the entire load range;
3. Acceptable tailpipe total hydrocarbon (THC) and CO emissions;
4. Robust performance during highly dynamic drive cycles and varying ambient conditions.

New hardware developments will play an important role in creating the desired in-cylinder conditions for ultra clean and efficient RCCI operations. This includes new fueling and air management hardware, such as direct injection dual-fuel injection, advanced turbocharging, variable valve actuation, and new after-treatment technologies. To guarantee robust and stable engine operations, advanced combustion control concepts are essential [6,7].

1.2. RCCI Control Challenges

RCCI is a pre-mixed combustion concept, which is characterized by controlled auto-ignition of the in-cylinder mixture. By early fuel injection that ends well before the start of combustion, sufficient mixing of the fresh air, injected fuels, and combustion products from previous cycles is achieved.

RCCI control is a relatively new research field and only a few experimental studies have been reported in the open literature up to now [8–14]. Table 1 summarizes their main control-related characteristics. To compensate for the effect of disturbances on the combustion process, these studies typically apply next-cycle fuel path control for individual cylinder control of the combustion phasing (CA50) or engine work (IMEP). Using this next-cycle control approach, combustion stability is improved by minimizing cyclic variability. By implementing a next-cycle controller for each cylinder, cylinder-to-cylinder variations are reduced and cylinder balancing is realized.

In most cases, PID controllers are applied. For example, Strandh et al. [9] compared the performance of a CA50 PID and a CA50 LQG controller on a six cylinder heavy-duty engine. For this single-input single-output (SISO) controller, good reference tracking, and good disturbance rejection for changes in engine speed and injected fuel energy is shown. However, in the multiple-input multiple-output (MIMO) case, coupling can be encountered between the fuel control loops, as illustrated in [11,12,15]. This limits the control performance. In [13], a model-predictive controller (MPC) with a five-cycle prediction horizon is implemented to control CA50 and IMEP. Using a physics-based combustion model, stable combustion and good tracking performance were demonstrated

for the load steps. MPC can deal with MIMO systems and can explicitly handle constraints, but it is more computationally expensive and sets more challenging control hardware requirements compared to PID control.

Table 1. Overview of experimental RCCI control studies. Abbreviations: FR—(mass- or energy-based) fuel ratio; CC—combustion centroid; MFB—mass fraction burned; DI—direct injection; SOI—start of injection; ω_e—engine speed; Q_f—fuel quantity; E_f—fuel energy).

Ref.	Controlled Parameter	Control Input	Control Strategy	Change or Disturbance
[8]	CA50, IMEPn	$Q_{f,tot}$, FR	PID	ω_e, IMEPn
[9]	CA50	FR	PID, LQG	ω_e, E_f
[10]	CA50	FR	PID	BMEP
[11]	CA50, IMEP	E_f, FR	PID	IMEP
[12]	MFB50, IMEP	$Q_{f,tot}$, FR or SOI_{DI}	PI	IMEP
[13]	CA50, IMEP	$Q_{f,tot}$, FR or SOI_{DI}	MPC	IMEP
[14]	CC, IMEP, PPR	$Q_{f,tot}$, $Q_{DI,post}$, FR, $SOI_{DI,post}$	PI	IMEP

For RCCI transient operation, studies focus on reference tracking of combustion parameters by fuel path control during the engine speed or load changes [8–13]. As illustrated in [10], PPR and NO emissions increased when CA50 was closed-loop controlled. However, realization of the desired emissions at maximum thermal efficiency while simultaneously guaranteeing safe and stable combustion is essential for real-world implementation. This requires accurate coordination of both air and fuel path to achieve the desired in-cylinder conditions. This is also crucial for combustion mode switching to cover the entire load range [6,14]; the diesel-E85 RCCI operation with a maximal gross IMEP between 9 [5,16] and 16.5 bar [17] is found. For a high load operation up to BMEP = 20 bar, conventional dual fuel mode with late injection timing needs to be applied, see e.g., [18]. To switch between these combustion modes, accurate air–fuel path control is key to realizing a smooth transition between the different operating conditions.

1.3. Research Objective and Main Contributions

Robust air–fuel path control is essential for real-world implementation of the RCCI combustion concept. Thus far, RCCI control studies focused on fuel path control only, as illustrated in Table 1, and the applied next-cycle PID controllers are manually tuned. This is typically done by studying the controlled RCCI engine behavior around a single operating point. Consequently, we aimed to develop a systematic control design approach that guarantees stable and robust RCCI performance under disturbances for coordinated air–fuel path control. This is a challenging control problem due to its complexity and coupling between the fuel and air path control loops.

In this work, a frequency domain-based control design method is proposed for the multi-variable RCCI engine control problem. This data-driven method combines frequency response function (FRF) system identification, system analysis, and feedback control design using loop shaping. With this method, allowable ranges in variations in combustion behavior and effective rejection of external disturbances can be specified for stable engine performance. Similar to [15,19], the proposed MIMO feedback controller combines linear parameter-varying (LPV) static decoupling with a diagonal PI feedback controller. Both studies concentrated on next-cycle control functionality and transient performance. Compared to these earlier studies, the main contributions of this work are:

- **A new, data-driven combustion uncertainty model** based on individual cylinder FRF system identification. This model quantifies the cylinder-to-cylinder variations;
- **Robust MIMO feedback control design** using the developed uncertainty model. This allows for a systematic trade-off between fast and robust performance for all cylinders;

- **Additional control design details on achieved input–output decoupling and robust stability**. This includes air–fuel path interaction analysis and robust stability analysis of the single feedback controller for varying operating points;
- **New experimental results for the six-cylinder diesel-E85 RCCI engine around three operating points;** in addition to earlier transient results, the potential of the RCCI engine controller is demonstrated to compensate for disturbed intake manifold temperature and to increase the high load RCCI range due to the reduced cylinder-to-cylinder variations.

This work is organized as follows. Firstly, the experimental set-up is introduced. Secondly, the RCCI control problem and the proposed RCCI engine control architecture are addressed in Section 3. Thirdly, Section 4 provides details on the systematic control design approach. For the developed controller, experimental results are presented and discussed in Section 5. Finally, the main conclusions and directions for future research are summarized.

2. Experimental Setup

Figure 1 shows a scheme of the studied heavy-duty engine platform, which is based on a modern, six-cylinder EURO-VI diesel engine. This standard production engine is equipped with a common rail direct injection (DI) system for diesel and a cooled, high-pressure exhaust gas recirculation (EGR) system. For advanced dual fuel RCCI research, the following hardware changes are implemented:

- E85 injection system with port fuel injection (PFI) for all cylinders as well as single point injection (SPI) capability;
- Modified piston;
- Modified turbocharger with a variable geometry turbine (VGT);
- Pressure sensor in each cylinder.

Implementation of the SPI system required an adaptation of the EGR system; a 4 kW electric heater and mixer with six injectors equally distributed around the circumference are installed downstream of the EGR cooler. The E85 fuel quantity injected in the EGR flow can mix with (fresh) air flow, which results in a homogeneous mixture of fuel, air, and combustion products from previous cycles in the intake manifold. By adding PFI capability, we can compensate for uneven mixture distribution over the cylinders. It is noted that the baseline common rail diesel injection system remained unchanged. The main engine specifications are listed in Table 2.

Table 2. Dual fuel RCCI engine specifications.

Parameter	Unit	Value or Spec
Number of cylinders	-	6 (in line)
Total displacement volume	ℓ	13
Compression ratio	-	15:1
DI fuel rail pressure	bar	500
PFI/SPI fuel rail pressure	bar	4.5
DI fuel	-	Diesel (EN590)
PFI/SPI fuel	-	E85

2.1. Data Acquisition

Engine performance is analyzed using various temperature, pressure, mass flow, and rotational speed sensors. In addition, post-turbine gaseous emissions are measured by a Horiba MEXA-ONE unit. These signals are sampled at 10 Hz by the engine test bed automation system.

For combustion analysis, an AVL Indimodul 621 in combination with Kistler 2853 charge amplifiers are available. This engine indication system acquires both crank angle data from

an AVL 365x pulse system and data from the Kistler 6125C in-cylinder pressure sensors at 0.1 deg CA resolution.

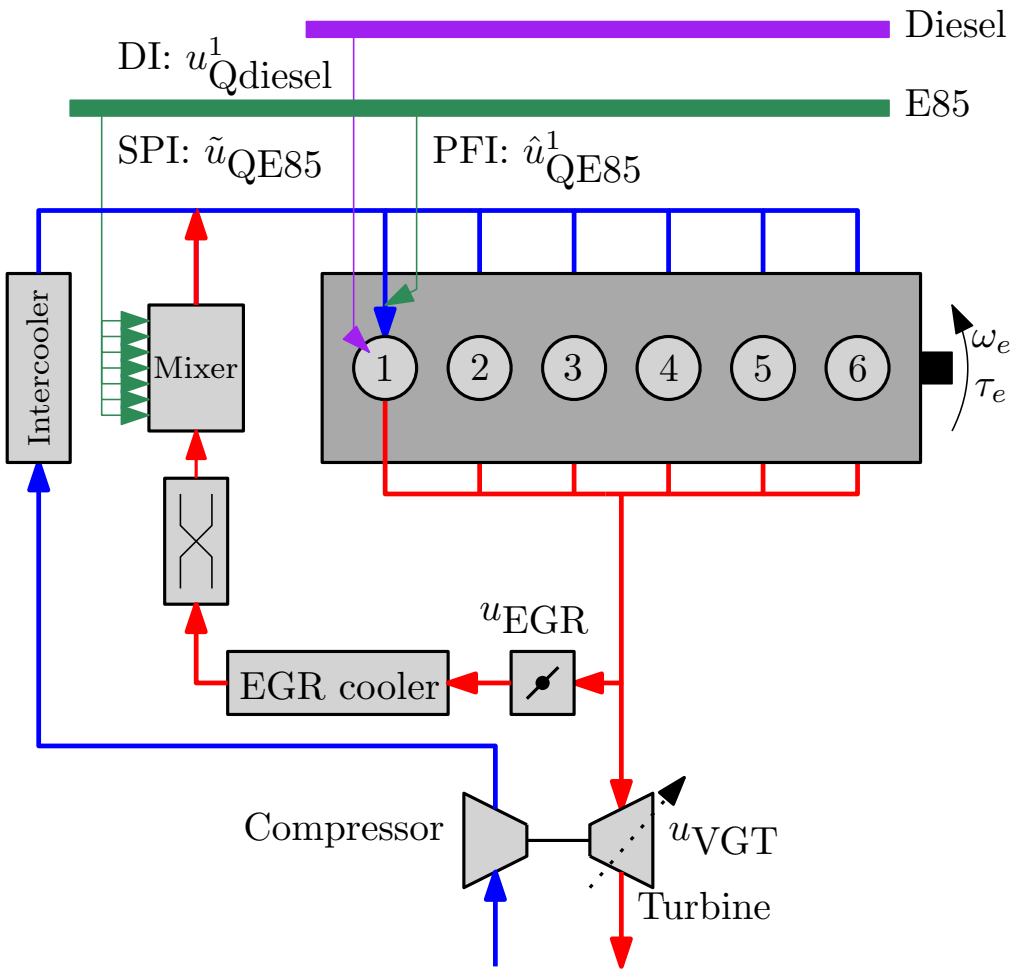

Figure 1. Scheme of the studied dual fuel RCCI engine with both diesel (purple) and E85 (green) fuel paths illustrated for cylinder 1 only.

2.2. Real-Time Control System

The standard engine control system is modified to create the desired flexibility to implement the developed RCCI control strategy. Besides the discussed engine hardware modifications, new control hardware is connected, as illustrated in Figure 2. This results in the following distributed control architecture. A Speedgoat rapid prototyping platform is selected to meet the challenging requirements for next-cycle combustion control. This platform consists of a Kintex 7 FPGA and an Intel Core i7 3.5 GHz CPU with two cores. The FPGA part serves for real-time and parallel processing of the in-cylinder pressure signals. For each combustion cycle, cylinder-individual combustion phasing (CA50) and net indicated mean effective pressure (IMEPn) are derived. Together with additional measurements, the calculated combustion parameters are input to the air and fuel path control software, which runs on the CPU part at a sample frequency of $f_s = 100$ Hz. The determined control actions are sent from the Speedgoat system to two low-level component controllers:

- Wingmate ECU controls the E85 PFI and SPI injectors, such that the desired injection timing and quantity is realized;
- dSPACE MABXII realizes the desired VGT and EGR valve position and diesel injection timing and quantity for the individual cylinders.

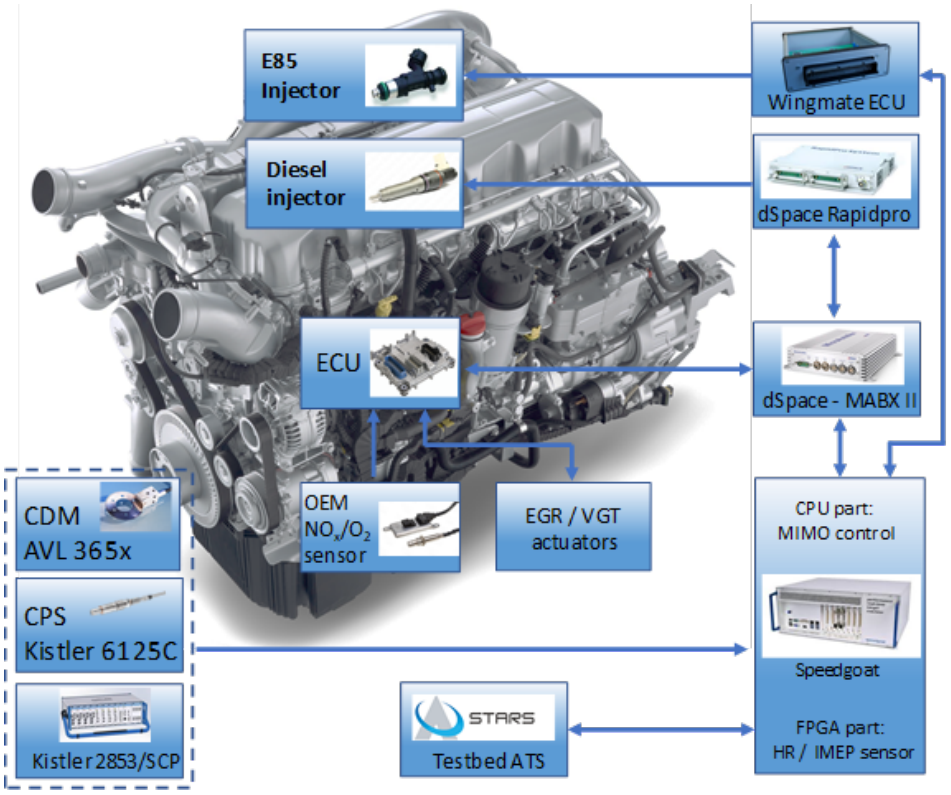

Figure 2. Overview of the hardware architecture of the implemented RCCI engine control system. Reprinted from [15] with permission. ©SAE International 2019.

2.3. Engine Operating Points

In this work, we concentrate on three engine operating points; around a central highway-like point (A), engine load (B), and engine speed (C) are varied. Based on extensive engine parameter sweeps, a trade off between high thermal efficiency and low engine out emissions is found within the constraints set by stable and safe operation. The corresponding optimal operational conditions are summarized in Table 3. More details on the selected engine control settings can be found in [15].

Table 3. Optimal RCCI operating conditions for the three studied points .

Parameter	Unit	A	B	C
Engine speed ω_e	rpm	1000	1000	1300
Net indicated mean effective pressure IMEPn	bar	8.5	11.5	8.5
Total injected E85 quantity u_{QE85}	mg/inj	136	180	125
Diesel DI injection quantity u_{QDiesel}	mg/inj	20.5	18.0	23.0
Diesel DI injection timing $u_{\mathrm{SOI\ Diesel}}$	deg CA aTDC	−40	−42	−40
E85 PFI injection timing $u_{\mathrm{SOI\ E85}}$	deg CA aTDC	−295	−295	−295
VGT position u_{VGT}	% open	38	35	56
EGR position u_{EGR}	% open	20	20	20
Energy-based blend ratio BR	%	81.8	87.0	78.6
Air fuel ratio λ_{AF}	-	2.3	2.2	2.5
Intake manifold pressure p_{im}	bar	1.98	2.40	2.05
Intake manifold temperature T_{im}	°C	32.5	34.0	32.0

3. RCCI Control

This section discusses the RCCI control problem and presents the proposed control system architecture. Details about the introduced feedforward and feedback controllers are given. This is essential input for the control design in Section 4.

3.1. RCCI Control Problem

The main objective of the RCCI engine controller is to realize the driver's power request with maximal fuel efficiency while meeting emission, safety and noise constraints. In this study, we focus on engine-out emissions. Table 4 lists the defined limits for safe and stable combustion. It is noted that the peak in-cylinder pressure rise rate is also associated with combustion noise.

Table 4. Limits for safe and stable RCCI operation.

Quantity	Limit
Peak in-cylinder pressure z_{PMAX}	200 bar
Peak in-cylinder pressure rise rate z_{PPR}	15 bar/deg CA
Combustion stability cov(IMEPn)	5%

Figure 3 shows a scheme of the studied RCCI engine with the proposed engine control system. The high level control objectives are indicated by:

$$z = \begin{bmatrix} z_\eta & z_{\mathrm{NO_x}} & z_{\mathrm{PM}} & z_{\mathrm{THC}} & z_{\mathrm{CO}} & z_{\mathrm{PMAX}} & z_{\mathrm{PPR}} \end{bmatrix}^\top, \tag{1}$$

with brake thermal efficiency z_η in %, nitrogen oxide emission $z_{\mathrm{NO_x}}$ in g/kWh, particulate matter emission z_{PM} in g/kWh, total hydrocarbon emission z_{THC} in g/kWh, and carbon monoxide emission z_{CO} in g/kWh. For the studied RCCI engine, the following control inputs are available to realize the desired in cylinder conditions:

$$u = \left[\begin{array}{ccc|cc} u^i_{\mathrm{QE85}} & u^i_{\mathrm{QDiesel}} & u^i_{\mathrm{SOI\ Diesel}} & u_{\mathrm{VGT}} & u_{\mathrm{EGR}} \end{array}\right]^\top, \tag{2}$$

where the VGT position u_{VGT} and EGR valve position u_{EGR} control the air and EGR flow into the cylinders. For fuel quantity and mixture control, E85 quantity u^i_{QE85}, diesel quantity u^i_{QDiesel}, and diesel injection timing $u^i_{\mathrm{SOI\ Diesel}}$ can be adjusted. As we have cylinder individual fueling capability, the cylinder number $i = \{1, 2, \ldots, 6\}$ is indicated. It is noted that u^i_{QE85} is a combination of the injected SPI quantity $\tilde{u}_{\mathrm{QE85}}$ and the cylinder individual injected PFI quantity $\hat{u}^i_{\mathrm{QE85}}$. This results in a total E85 fueling quantity per cylinder:

$$u^i_{\mathrm{QE85}} = \tilde{u}_{\mathrm{QE85}} + \hat{u}^i_{\mathrm{QE85}}. \tag{3}$$

For the presented experimental results, unless stated elsewhere, the applied total PFI-to-SPI E85 mass flow ratio is 50%:50%. For all ratios, the total injected E85 quantity, which is specified in Table 3, is always realized.

RCCI performance is very sensitive for variations in operating conditions, such as different duty cycles or varying ambient conditions. These external disturbances are given by:

$$w = \begin{bmatrix} \tau_{load} & \omega_e & p_a & T_a \end{bmatrix}^\top, \tag{4}$$

with engine load torque τ_{load} in Nm, engine speed ω_e in rpm, ambient pressure p_a in Pa and ambient temperature T_a in °C. Uncontrolled combustion can lead to misfires or partial combustion at low load, which is associated with high CO and HC emissions. At high loads, knocking and high peak cylinder pressures can be present. This has to be avoided, since it can result in engine damage and unacceptable noise levels. As a result, the main control challenge is to guarantee robust performance during real-world operations. This is essential to bring RCCI engines on the road.

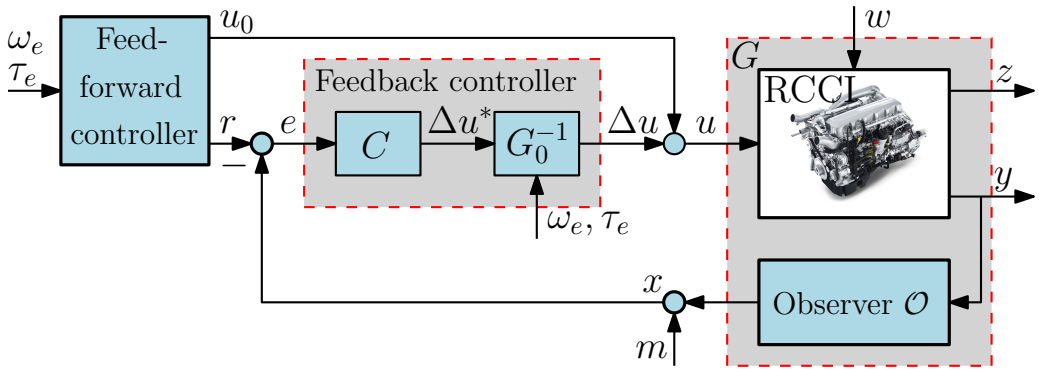

Figure 3. Scheme of the RCCI engine with the proposed control system architecture (adapted from [19]).

3.2. RCCI Engine Control Architecture

Similar to previous work [15,19], a combined feedforward–feedback control architecture is proposed to coordinate air and fuel path, see Figure 3. Nominal optimal performance is realized by the feedforward controller, whereas robust performance has to be guaranteed by the feedback controller based on real-time information from the observer $\mathcal{O}$ (also called virtual sensor). Using crank angle and in-cylinder pressure information, this observer determines crucial combustion parameters for engine load an combustion phasing control. In the proposed control strategy, cylinder individual, net indicated mean effective pressure (IMEPn) and the crank angle where 50% of the total heat is released (CA50) are calculated for each combustion cycle. Details about the implemented virtual sensor can be found in, e.g., [7]. In the "sequel" of this section, both controllers are discussed in more detail.

3.3. Feedforward Controller

For each engine speed ω_e and requested engine brake torque τ_e, the feedforward controller gives the nominal control input settings u_0 and corresponding reference values r. These values are determined during an off-line optimization process and give the best trade-off between brake thermal efficiency and engine out emissions. In the literature, various methods are proposed to determine these optimal engine settings, see e.g., [20,21].

As the high-level objectives z in (1) cannot be measured directly using production sensors, related quantities have to be selected. Based on the available observed signals x, correlations $z(x)$ and controllability of x, the following reference signals r are selected:

- **Net indicated mean effective pressure** (IMEPn) is a cylinder individual measure for engine load and is an indicator for misfires and partial combustion;
- **Energy-based blend-ratio** is defined as:

$$\mathrm{BR} = \frac{\dot{m}_{\mathrm{E85}} \mathrm{LHV}_{\mathrm{E85}}}{\dot{m}_{\mathrm{E85}} \mathrm{LHV}_{\mathrm{E85}} + \dot{m}_{\mathrm{diesel}} \mathrm{LHV}_{\mathrm{diesel}}} \cdot 100\%, \tag{5}$$

  where $\dot{m}$ denotes the cylinder individual mass flow and LHV the lower heating value of the fuel. This quantity has a strong link with THC and CO emissions and combustion stability;
- **Combustion phasing** (CA50) is an important indicator for the mixing period and for combustion stability. Moreover, CA50 is closely linked to thermal efficiency;
- **Exhaust manifold pressure** p_{em} is associated with EGR mass flow and pumping losses;
- **EGR ratio** is given by:

$$X_{EGR} = \frac{\dot{m}_{\mathrm{EGR}}}{\dot{m}_{\mathrm{EGR}} + \dot{m}_c} \cdot 100\%, \tag{6}$$

  with EGR mass flow $\dot{m}_{\mathrm{EGR}}$ and compressor fresh air flow $\dot{m}_c$. It is linked to the oxygen content in the intake manifold.

With the implemented in-cylinder pressure sensors, z_{PMAX} and z_{PPR} can be continuously monitored for each cylinder. However, they are not directly controlled; if a safety limit is violated, the engine controller switches to a fail safe operating mode. In this work, the RCCI control performance is also examined for a dynamic test cycle, which is characterized by engine load and speed variations. In that case, the feedforward controller linearly interpolates between the calibrated values in the 2D look-up tables $u_0(\omega_e, \tau_e)$ and $r(\omega_e, \tau_e)$.

3.4. Multivariable Feedback Controller

To track the desired reference values r, a static decoupling matrix G_0^{-1} is combined with a diagonal feedback controller C. The resulting multivariable feedback controller is easy to implement on a production ECU. Assuming that the static decoupling is effective, all fuel and air path feedback control loops can be treated independently. For these loops, five proportional integral (PI) controllers are implemented, which leads to the diagonal feedback controller:

$$C = \left[\begin{array}{c|c} \mathrm{PI}_{\mathrm{fuel}} & 0 \\ \hline 0 & \mathrm{PI}_{\mathrm{air}} \end{array}\right], \tag{7}$$

$$= \left[\begin{array}{ccc|cc} c_{\mathrm{IMEPn}} & 0 & 0 & 0 & 0 \\ 0 & c_{\mathrm{BR}} & 0 & 0 & 0 \\ 0 & 0 & c_{\mathrm{CA50}} & 0 & 0 \\ \hline 0 & 0 & 0 & c_{\mathrm{pem}} & 0 \\ 0 & 0 & 0 & 0 & c_{\mathrm{EGR\ ratio}} \end{array}\right], \tag{8}$$

The subscripts indicate the controlled reference signal; e.g., c_{IMEPn} is the IMEPn controller.

3.4.1. Next-Cycle Fuel Path Control

To deal with cylinder individual cyclic variations as well as cylinder-to-cylinder variations, combustion phasing, and heat release control are key for stable and safe RCCI combustion. Moreover, the blend ratio BR has to be kept at its desired value. Therefore, next-cycle PI control is applied for the three fuel path controllers $c_{\mathrm{IMEPn}}, c_{\mathrm{BR}}$, and c_{CA50}. This is implemented using a forward Euler integration scheme:

$$\Delta u^i[k] = \Delta u^i[k-1] + K_P e^i[k-1] + K_I T_{\mathrm{cycle}} e^i[k-2], \tag{9}$$

where $e^i[k] = r[k] - x^i[k]$ is the reference tracking error for combustion cycle k, and T_{cycle} is the combustion cycle time. It is noted that the (variable) update frequency of the next-cycle fuel path controller is set by the engine speed ω_e (in rpm). As seen from Section 3.3, the selected observed outputs are:

$$x^i = \left[\begin{array}{ccc|cc} x^i_{\mathrm{IMEPn}} & x^i_{\mathrm{BR}} & x^i_{\mathrm{CA50}} & x_{\mathrm{pem}} & x_{\mathrm{EGR}} \end{array}\right]^\top, \tag{10}$$

Each individual cylinder is controlled by the corresponding three fuel path controllers. For ease of implementation, identical references r and control parameters K_P and K_I are used for the different cylinders. Therefore, the superscript i is omitted for these quantities.

3.4.2. Air Path Control

Two SISO PI controllers control the exhaust manifold pressure and the EGR ratio, respectively. Both controllers are running in the time domain and operate with an update frequency of f_s. Typically, the air path dynamics are significantly slower than the fuel path dynamics. This limits the maximum closed-loop bandwidth of the air path controllers.

4. Feedback Control Design

For the design of a robust RCCI engine feedback controller, a model-based approach is followed. This approach relies on frequency domain-based analyses and is characterized by three main steps:

1. Multiple-input multiple-output (MIMO) system identification;
2. Static decoupling design;
3. Robust loop shaping using a combustion uncertainty model;

These steps are discussed in more detail.

4.1. MIMO System Identification

As illustrated in Figure 3, we aim to develop a controller for the RCCI engine with observer $\mathcal{O}$, which is indicated as plant G. To do so, a data-driven model is identified by determining the frequency response function (FRF) [22]. With this method, we are able to identify cylinder individual combustion models. Moreover, the behavior of the observer and actuator and sensor dynamics are included. First, multi-sine excitation signals are applied to each individual control input u and the resulting outputs x are recorded. Secondly, a single-input multiple-output (SIMO) system model is identified. Thirdly, by combining the results for all individual control inputs, a square frequency response function matrix for the overall multiple-input multiple-output (MIMO) system is found:

$$G_q(j\omega) = \frac{X(j\omega)}{U(j\omega)} = \left[\begin{array}{c|c} G^i_{\text{inj-comb}} & G^i_{\text{valve-comb}} \\ \hline G_{\text{inj-air}} & G_{\text{valve-air}} \end{array}\right], \quad q = \{\text{A}, \text{B}, \text{C}\}. \tag{11}$$

Consequently, three unique, linear plant models $G_q(j\omega)$, which capture the local system behavior, can be identified. Figure 4 shows the resulting FRF matrix for operating point A. In these experiments, we applied a zero-mean, multi-sine excitation u with random phase and 800 s duration. Excitation frequencies are chosen between 0.02 Hz and 10 Hz. Element g_{mn} of this matrix is the FRF, which corresponds to the m observed output (mentioned for each row) and the n control input (mentioned above each column). In the upper part of this figure, cylinder individual FRFs for $G^i_{\text{inj-comb}}$ and $G^i_{\text{valves-comb}}$ are plotted. It clearly illustrates that the combustion behavior varies for the six cylinders. This is attributed to the unequal distribution of the fresh air, EGR and SPI E85 mixture over the cylinders. Moreover, different cylinder wall temperatures can cause these variations, especially for the two outer cylinders. For the air path response, which is shown in the lower part of the figure, only a single (engine mean) response exists.

4.2. Static Decoupling Design

Using the data-driven, linear models $G_q(j\omega)$, a static decoupling matrix $G^{-1}_{q,0}$ is designed for the individual operating points, such that we obtain the new, decoupled system:

$$\bar{G}_q(j\omega) = \frac{X(j\omega)}{U^*(j\omega)} = G_q(j\omega)G^{-1}_{q,0}, \quad q = \{\text{A}, \text{B}, \text{C}\}. \tag{12}$$

The decoupling matrix is the inverse of the static gain matrix $G_{q,0}$. This matrix is approximated by taking the average magnitude $|G_q(j\omega)|$ for low frequencies.

The sign of the constant elements of $G_{q,0}$ is determined by the corresponding phase of $G_q(j\omega)$. A phase of 0 deg results in a positive sign of the element $g_{0,mn}$, whereas a phase of -180 deg results in a negative sign. For ease of implementation, we define one decoupling matrix for all six cylinders. This is done by applying the static decoupling matrix of cylinder 1 to all cylinders. For operating point A, this results in:

$$G^{-1}_{\text{A},0} = \begin{bmatrix} 13.021 & 2.221 & -0.996 & 0.03 & 0.161 \\ 1.986 & -1.051 & -0.152 & 0.005 & 0.024 \\ 2.740 & -1.193 & 1.192 & 0.021 & 0.103 \\ 2.043 & -0.146 & -0.095 & -0.128 & -0.629 \\ 5.014 & -0.359 & -0.234 & -0.314 & 2.091 \end{bmatrix}. \tag{13}$$

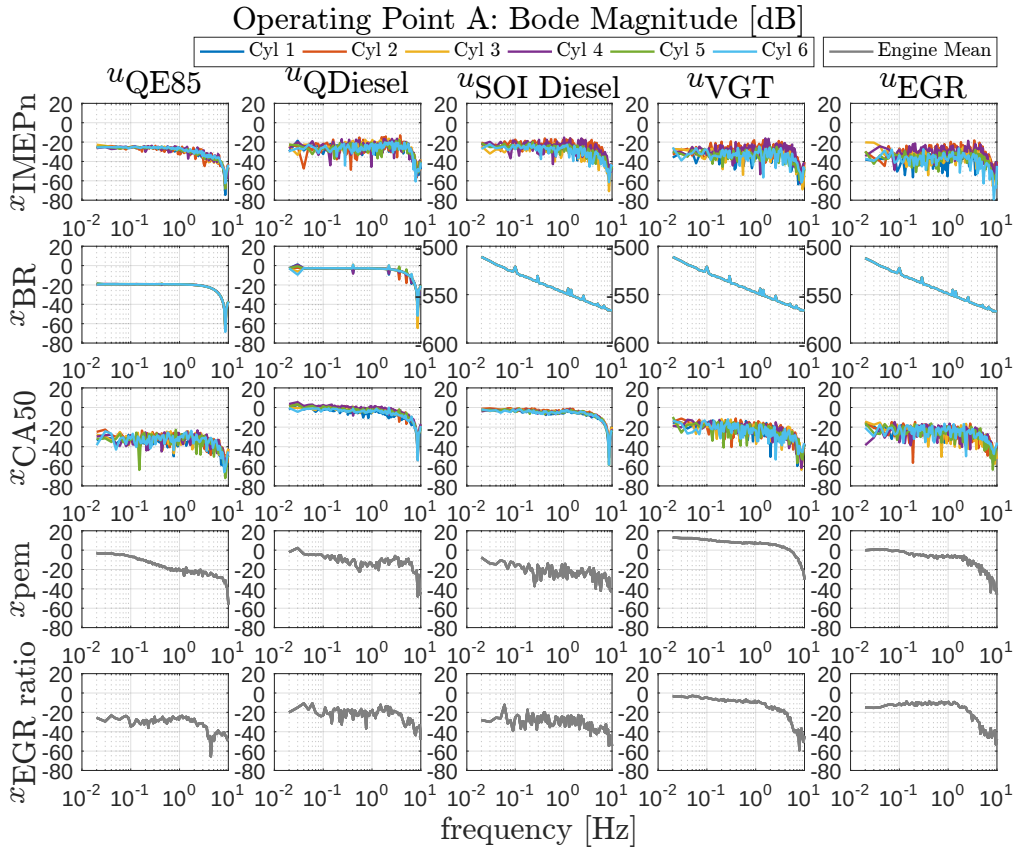

Figure 4. MIMO system identification results for operating point A. Reprinted from [19] with permission of the International Federation of Automatic Control 2020.

As illustrated in Figure 3, this part of the controller determines new control inputs Δu^*, which are a linear combination of the available control inputs in (2). In other words, decoupling is effectively realized by coordination of the air and fuel path. During transient operation, the values of the local static decoupling matrices $G_{q,0}^{-1}$ are scheduled as a function of engine speed ω_e and requested engine load τ_e.

In order to assess the effectiveness of the static decoupling, an interaction analysis is performed using the relative gain array (RGA) [23]. The RGA of the decoupled system is defined as:

$$\mathrm{RGA}(\bar{G}_q) = \bar{G}_q \times (\bar{G}_q^{-1})^\top, \quad q = \{\mathrm{A}, \mathrm{B}, \mathrm{C}\}. \tag{14}$$

If the RGA is close to the identity matrix I, the system is dynamically decoupled.

In Figure 5, the results for all elements of $\mathrm{RGA}(\bar{G}_q)$ are summarized for operating point A. Note that this is done for the individual cylinders. The terms of the diagonal elements are found to be close to 0 dB for frequencies up to approximately 0.4 Hz. In this frequency window, the terms of the off-diagonal elements are negligible, i.e., close to -30 dB. Consequently, decentralized controller design for the decoupled system $\bar{G}$ is expected to be effective up to a bandwidth of 0.4 Hz. In line with expectations, at higher frequencies (above 5 Hz), the static decoupling is less effective. Similar results are found for operating point B and C.

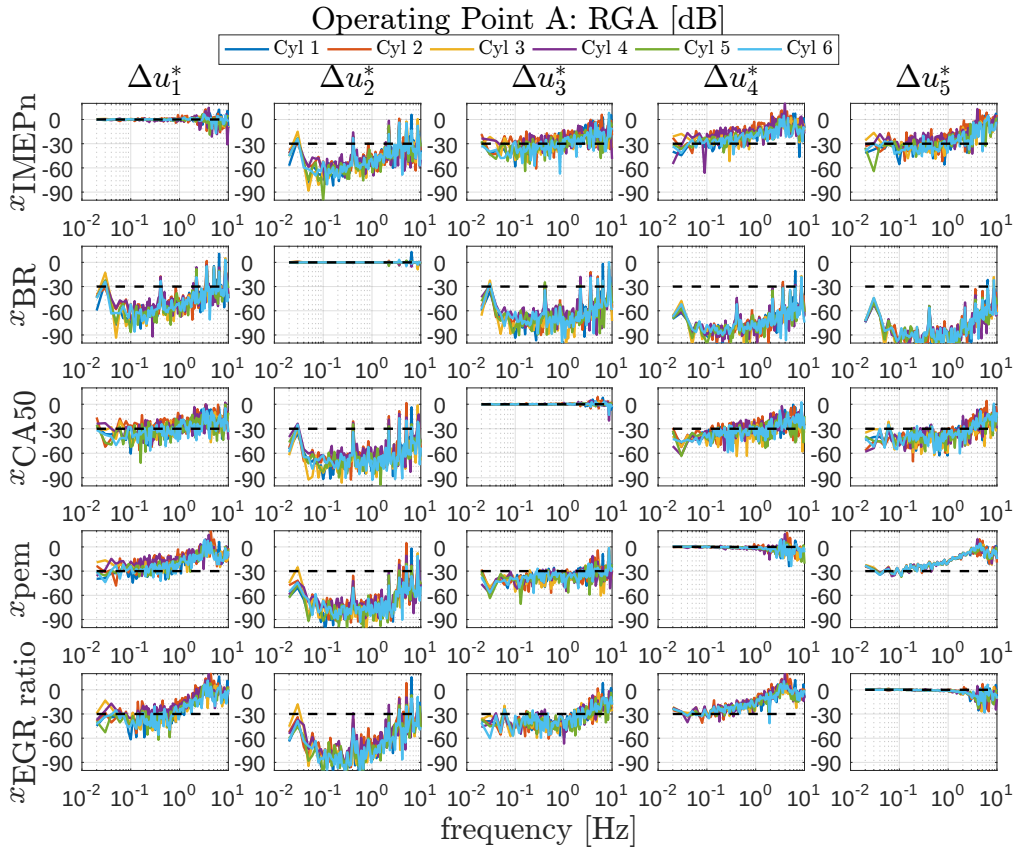

Figure 5. Results of the interaction analysis for decoupled plant $\bar{G}_q(j\omega)$ in operating point A.

4.3. Robust Loop Shaping

Assuming an effective decoupling, the MIMO feedback control design reduces to the design of five independent SISO feedback controllers, as described in (8). In this work, we aim to determine one unique controller C for all three operating points, such that control implementation and calibration effort is minimized. To guarantee stable and robust performance for all three operating points, first a dynamic uncertainty model is derived for the decoupled system $\bar{G}_q$. Based on this model, a robust design is determined for the five SISO controller using frequency-domain loop-shaping. These two steps are discussed in more detail and are illustrated for the design of c_{IMEPn}.

4.3.1. Dynamic Uncertainty Model

To deal with cylinder-to-cylinder variations, a multiplicative, dynamic uncertainty model is introduced:

$$\tilde{G}_q(s) = \tilde{G}_{q,\mathrm{nom}}(s)[1 + \Delta\tilde{G}(s)]. \tag{15}$$

with nominal plant model $\tilde{G}_{q,\mathrm{nom}}(s)$ and dynamic uncertainty model $\Delta\tilde{G}(s)$ For control design, only the diagonal terms of $\tilde{G}_q(s)$ are of interest: i.e., $\tilde{g}_{q,jj}$ with $j = \{1,2,\ldots,5\}$. Then, (15) boils down to:

$$\tilde{g}_{q,jj}(s) = \tilde{g}_{q,jj,\mathrm{nom}}(s)[1 + \Delta\tilde{g}_{jj}(s)], \tag{16}$$

where the nominal plant model consists of two parts:

$$\tilde{g}_{q,jj,\mathrm{nom}}(s) = \mathrm{ZOH}_q(s)F_q(s), \tag{17}$$

with:

$$\mathrm{ZOH}_q(s) = \frac{1 - e^{-T_{\mathrm{cycle}}s}}{T_{\mathrm{cycle}}s}, \tag{18}$$

$$F_q(s) = \frac{a}{s+b} e^{-T_{\text{cycle}} s}. \tag{19}$$

The zero-order-hold model ZOH(s) is required, since the control are updated after each combustion cycle. It is noted that the model parameter T_{cycle} depends on the engine speed: $T_{\text{cycle}} = (2 \times 60)/\omega_e$.

The combustion physics $F_q(s)$ are approximated by a first-order model with an engine speed dependent input delay. From additional experiments, it is concluded that these combustion physics are associated with wall-wetting effects. This is in line with the results in [24]. The dynamic multiplicative uncertainty in (16) is modeled as an operating point independent skewed-notch filter:

$$\Delta\tilde{g}_{jj}(s) = c \left(\frac{\frac{s^2}{(\omega_1)^2} - \frac{\beta_1}{\omega_1} s + 1}{\frac{s^2}{(\omega_2)^2} + \frac{\beta_2}{\omega_2} s + 1} \right). \tag{20}$$

This approach is illustrated for the identification of a dynamic uncertainty model for the first decoupled diagonal term $j = 1$ and all operating points $q = \{\text{A}, \text{B}, \text{C}\}$, so $\bar{g}_{q,11}(j\omega)$. The described steps are also applicable to the other diagonal terms of $\bar{G}_q$. First, the nominal plant model is identified by solving a least square optimization problem. The resulting model parameters are listed in Table 5.

Table 5. Nominal plant model $\tilde{g}_{q,11,\text{nom}}$ parameters.

Operating Point q	ω_e [rpm]	T_{cycle} [s]	a	b
A	1000	0.1200	6.745	6.745
B	1000	0.1200	6.745	6.745
C	1300	0.0923	10.321	10.321

Having identified the nominal plant model, the next step is to identify the dynamic uncertainty model (20). Therefore, model parameters are determined, which satisfy the following relation:

$$\left| \frac{\bar{g}_{q,jj}(j\omega)}{\tilde{g}_{q,jj,\text{nom}}(j\omega)} - 1 \right| \leq |\Delta\tilde{g}_{jj}(j\omega)|. \tag{21}$$

For $q = \{\text{A}, \text{B}, \text{C}\}$ and $j = 1$, the following parameters are found: $c = 0.5$, $\beta_1 = 2$, $\beta_2 = 2$, $f_1 = \frac{\omega_1}{2\pi} = 1.8$ Hz and $f_2 = \frac{\omega_1}{2\pi} = 50$ Hz. This gives the uncertainty model $\Delta\tilde{g}_{11}$, which is plotted in Figure 6. For reference, the individual cylinder deviations from the nominal model in operating point A are also shown. It is seen that, up to 1 Hz, this model gives a good approximation of the upper bound on the magnitude of the decoupled plant of all cylinders.

4.3.2. SISO Feedback Controller Design

To control the RCCI engine with static decoupling, five parallel PI controllers have to be designed, as described by (8):

$$c_j(s) = \frac{K_P s + K_I}{s}. \tag{22}$$

The two air path controllers are extended with a first order low-pass filter with cut-off frequency $f_{LP} = \frac{1}{2\pi\tau_{LP}}$ to filter out high-frequent measurement noise. Note that a single controller c_j is used for all operating points $q = \{\text{A}, \text{B}, \text{C}\}$.

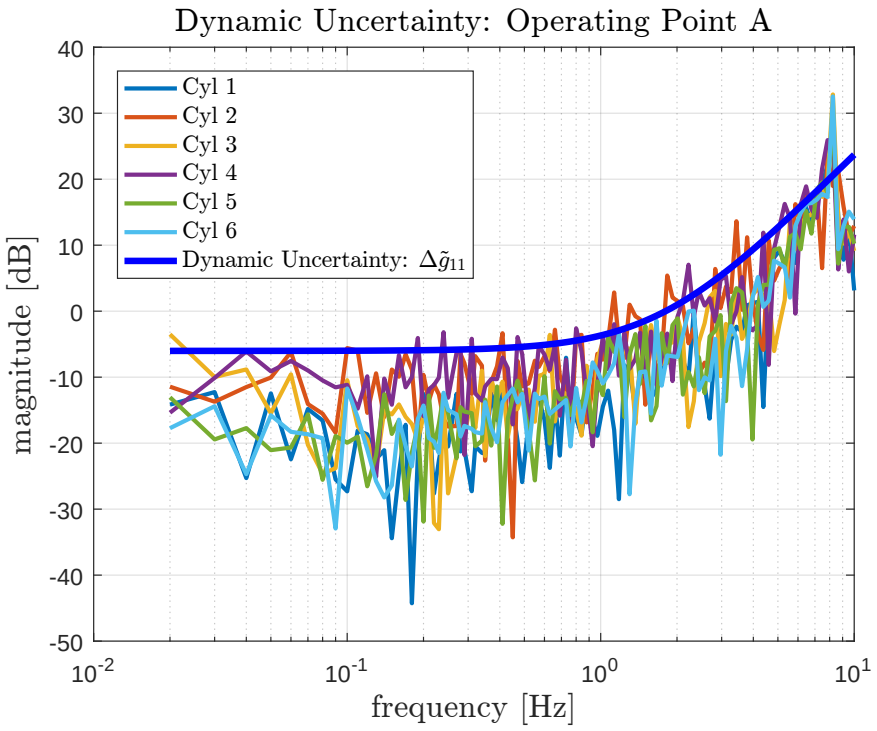

Figure 6. Dynamic combustion uncertainty model $\Delta\tilde{g}_{11}$.

For RCCI engine control design, it is important to explicitly deal with the effect of system uncertainty and external disturbances on engine performance. Therefore, frequency-domain loop shaping is applied. By assuming effective decoupling, SISO system analysis is performed. Based on analysis of the loop gain $l_{q,jj} = \tilde{g}_{q,jj}c_j$, this systematic method gives clear requirements for stable and robust RCCI engine operation. SISO stability can easily be assessed from the Nyquist plot. To guarantee robust performance, the Gain Margin (GM), Phase Margin (PM) and Modulus Margin (MM) are specified, see Figure 7. The targeted values are summarized in the top of Table 6. More details about this loop shaping method can be found in [23].

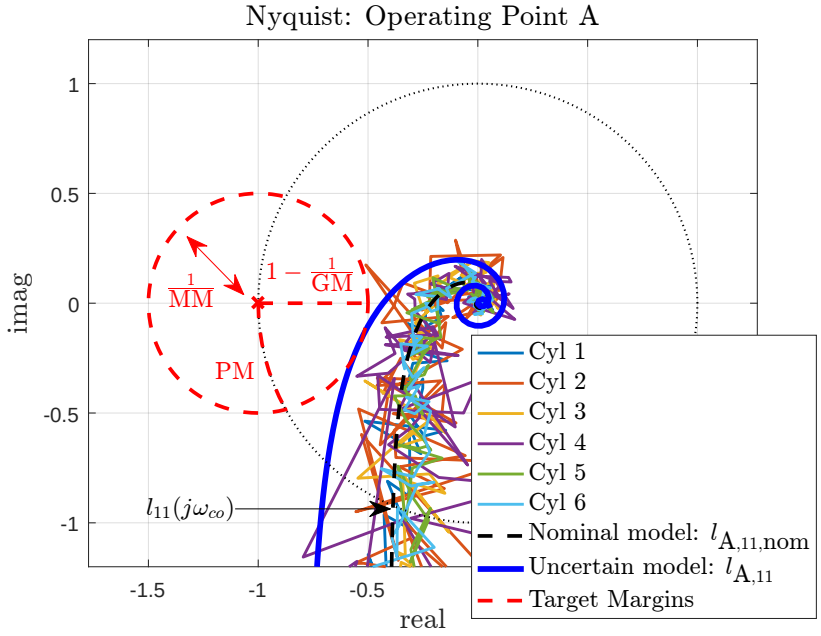

Figure 7. Nyquist plot of loop gain $l_{A,11}$ for six individual cylinders (operating point A).

Table 6. Performance indicators and robustness margins of the five SISO feedback controllers for operating points A, B, and C.

Output	Resp. Time [cycles]	ω_{co} [Hz]	PM [deg]	GM [dB]	MM [dB]
Design Target			**PM** $>$ **30**	**GM** $>$ **6**	**MM** $<$ **6**
		Operating point A			
x_{IMEPn}	8	0.27	86.5	14.5	2.5
x_{BR}	11	0.32	97.8	inf	0.5
x_{CA50}	9	0.26	77.2	15.6	1.6
x_{pem}	32	0.10	76.5	13.6	2.1
$x_{\text{EGR ratio}}$	28	0.11	94.1	6.4	5.6
		Operating point B			
x_{IMEPn}	8	0.32	70.6	11.2	3.2
x_{BR}	12	0.32	97.8	Inf	0.5
x_{CA50}	10	0.30	78.9	16.3	1.7
x_{pem}	29	0.10	83.3	12.6	2.4
$x_{\text{EGR ratio}}$	35	0.12	94.2	6.4	5.6
		Operating point C			
x_{IMEPn}	10	0.30	79.4	16.4	1.8
x_{BR}	11	0.32	99.5	Inf	0.4
x_{CA50}	10	0.24	75.4	18.1	1.2
x_{pem}	25	0.10	74.6	15.1	1.7
$x_{\text{EGR ratio}}$	30	0.13	95.6	7.9	5.0

Using the uncertainty model, the feedback controller can be designed more systematically and efficiently; if the robustness margins are met for the uncertainty model, the individual cylinder controllers also satisfy the design criteria. More precisely, the loop gain $l_{q,jj}(j\omega) = \tilde{g}_{q,jj}(j\omega)c_j(j\omega)$ is shaped for closed-loop stability, while dealing with robustness margins and performance. The latter is expressed by the cross-over frequency ω_{co}, which is a measure for the closed-loop bandwidth [23]. The applied control settings and resulting robustness margins are listed in Table 6 and Table 7, respectively. For operating point A, the corresponding Nyquist plot of $l_{\text{A},11}$ is shown in Figure 7 for the next-cycle IMEPn controller. The model including uncertainty (in blue) clearly respects the target robustness margins. As illustrated in this figure, the six cylinder individual controllers also meet these robust performance criteria for these control settings. From additional analysis, it is also concluded that the designed controllers have good disturbance rejection properties, see also [19]. The Nyquist plot of $l_{\text{B},11}$ and $l_{\text{C},11}$ can be found in Appendix A. These figures illustrate that the stability criterion as well as the target robustness margins are met for all studied operating points. It is noted that the stability of the five-by-five closed-loop MIMO system can be analyzed by studying the characteristic loci, see e.g., [23]. This analysis also proofed that the closed-loop MIMO system is stable.

Table 7. Control parameter settings for SISO fuel- and air-path controllers.

SISO Controller	K_P	K_I	τ_{LP} [s]
c_{IMEPn}	0.25	2.00	n/a
c_{BR}	0.25	2.00	n/a
c_{CA50}	0.25	2.00	n/a
c_{pem}	0.5	0.79	0.0159
$c_{\text{EGR ratio}}$	0.5	0.79	0.0159

Besides robust performance, the reference tracking performance of the feedback controller is important, especially during transients. Therefore, the response time is included in Table 6. It is defined as the number of combustion cycles needed by the output x to

reach 90% of the reference input step r. From this table, we conclude that the cylinder individual combustion parameters are controlled relatively fast; an increase of 1 bar in r_{IMEPn} is realized in 8 engine cycles. For step wise changes in r_{CA50}, a response time of 10 cycles is observed. Both response times are larger than the values found in literature for the best tracking performance: 1 to 4 cycles for IMEP control [12,14] and 3 cycles for CA50 control [9]. This difference is mainly contributed to the controller calibration; in the trade-off between robustness and performance, current robustness margins still leave room for further performance improvement, see Table 6. However, wall wetting effects will remain a limiting factor; with an estimated delay in the combustion physics $F_q(s)$ of 0.12 s, it takes one cycle before the output x starts to respond to PFI E85 changes. Together with the delay due to next-cycle control updates, this means that a minimal IMEP response time of two engine cycles is expected in the studied engine. Moreover, the relatively slow air path dynamics strongly affect the response time of x_{pem} and $x_{\text{EGR ratio}}$. These response times are on the order of 30 cycles, which is in line with values found in [10] for open-loop controlled system responses.

5. Experimental Results

The developed RCCI engine controller proved to enhance stable engine operation due to significant reduction of cylinder-to-cylinder variance in previous work [19]. This work concentrates on the demonstration of robust RCCI engine operation. Therefore, the RCCI engine controller's performance is studied for three different cases. Firstly, the transient performance of the controlled RCCI engine is studied for engine speed and engine load variations. Secondly, its capabilities to effectively reject the effect of unknown disturbances in operating conditions is examined. Here, the focus is on disturbed intake manifold temperature. Thirdly, results are presented that demonstrate the controller's potential to increase the RCCI load range due to enhanced stable and safe operation.

5.1. Transient RCCI Engine Performance

In automotive applications, future RCCI engines have to be able to deal with various dynamic duty cycles. As a first step, the performance of the closed-loop controlled RCCI engine is examined for the test cycle shown in Figure 8. This cycle connects the three studied operating points via engine speed and engine load ramps.

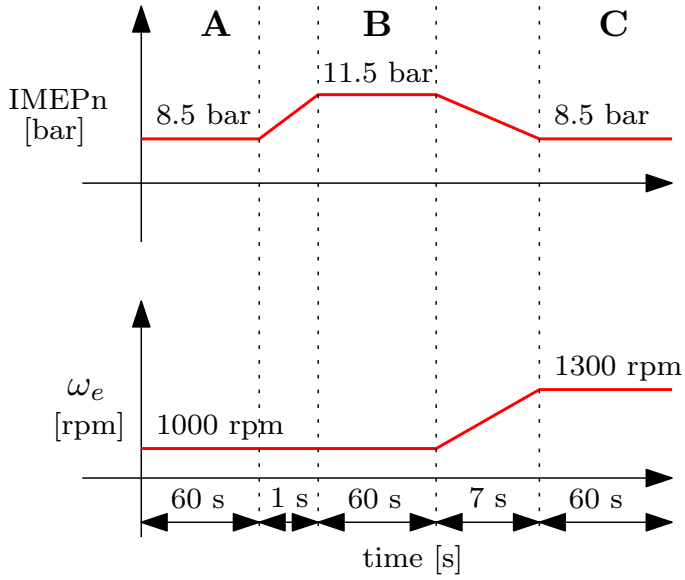

Figure 8. Test cycle around the three studied operating points for evaluation of transient RCCI engine performance. Reprinted from [19] with permission of the International Federation of Automatic Control 2020.

To assess the potential of the closed-loop controlled RCCI engine, its performance is compared with the open-loop control performance, i.e., RCCI engine with feedforward controller only. Figure 9 gives the experimental results for the control inputs u, observed outputs x and performance outputs z, respectively. The performance outputs include peak in-cylinder pressure z_{PMAX} , peak in-cylinder pressure rise rate z_{PPR} and engine out NO_x and THC emissions, z_{NOx} and z_{THC}, respectively. Although the cylinder individual feedback controllers are active in the closed-loop control case, cylinder-averaged fuel path control settings and cylinder-averaged combustion parameters are plotted. This is done for comparison purposes.

This figure clearly illustrates that the RCCI process is very sensitive for varying operating conditions. After changing the fuelling and air path settings around engine cycle 500, the observed outputs x differ from the desired reference values r in the open-loop control case. Especially, a drift in CA50 is observed, which converges to the desired stationary value in 500 engine cycles. This slow process is associated with engine heat up due to the increased engine load. As a result, in-cylinder temperatures increase, such that CA50 advances and both z_{PMAX} and z_{PPR} increase. For x_{IMEPn}, x_{pem}, and x_{EGR}, this initial offset does not reduce. Stationary operating conditions differ from the reference values for the open-loop control settings. During transients, peaks in x_{pem} and x_{EGR} are seen. This is mainly due to interaction between the fuel and air path control loops.

The closed-loop controller manages, after an initial offset, to control the observed outputs to their desired values. Due to their larger response time, this requires more combustion cycles for the air path parameters than for the combustion parameters. Test-averaged cov(IMEPn), which is a measure for combustion stability, is reduced from 6.0% in the open-loop control case down to 3.3%. Comparison of the reference r and the five observed outputs x learns that good tracking behavior is achieved due to accurate coordination of the air and fuel path settings by the closed-loop RCCI engine controller. It is concluded that effective input–output decoupling is achieved, since minimal interaction is seen between the control loops. As expected, larger deviations between r and x are seen during transients. The average absolute value and standard deviation of the cylinder-averaged tracking error are specified in Table 8. These cycle results illustrate that accurate reference tracking is not only realized during the studied stationary operating points, but also during the transient periods, where engine speed or engine load vary. The RCCI engine controller tracks x_{IMEPn} and x_{CA50} with average tracking errors of 0.24 bar and 0.45 deg CA, respectively. The results are in line with the best transient results presented in [13,14]: 0.15 bar and 1.4 deg CA. for $\bar{e}_{\mathrm{IMEPn}}$ and $\bar{e}_{\mathrm{CA50}}$, respectively, and 0.20 bar and 1.5 deg CA for σ_{IMEPn} and σ_{CA50}. However, in this study, the desired air path conditions are also closely followed by the coordinated air–fuel path controller. Especially, the peaks in x_{pem} and x_{EGR} during transients are reduced by the closed-loop controller. Although a higher NO_x peak is found due to reduced EGR ratios around engine cycle 1100, the test-averaged NO_x emission is reduced by 0.1 g/kWh (12.8%). At the same time, the test-averaged z_{PMAX} and z_{PPR} are reduced by 7.9 bar and 1.1 bar/deg CA and their peak values are cut by 14.4 bar and 3.8 bar/deg CA, respectively. Partly, the reductions are explained by the reduced diesel and E85 fuel quantity to realize the reduced IMEPn reference values. This is also assumed to be key in the overall reductions of z_{PMAX} and z_{PPR}. Besides fuelling, combustion phasing strongly affects these values between engine cycle 500 and 1000. Over the entire test cycle, tracking of x_{EGR} gives reduced EGR ratios. The corresponding increased Air Fuel ratios λ_{AF} lead to lower combustion temperatures. This explains the trend in test-averaged THC emissions: 1.2 g/kWh (12.6%) increase compared to the open-loop control case.

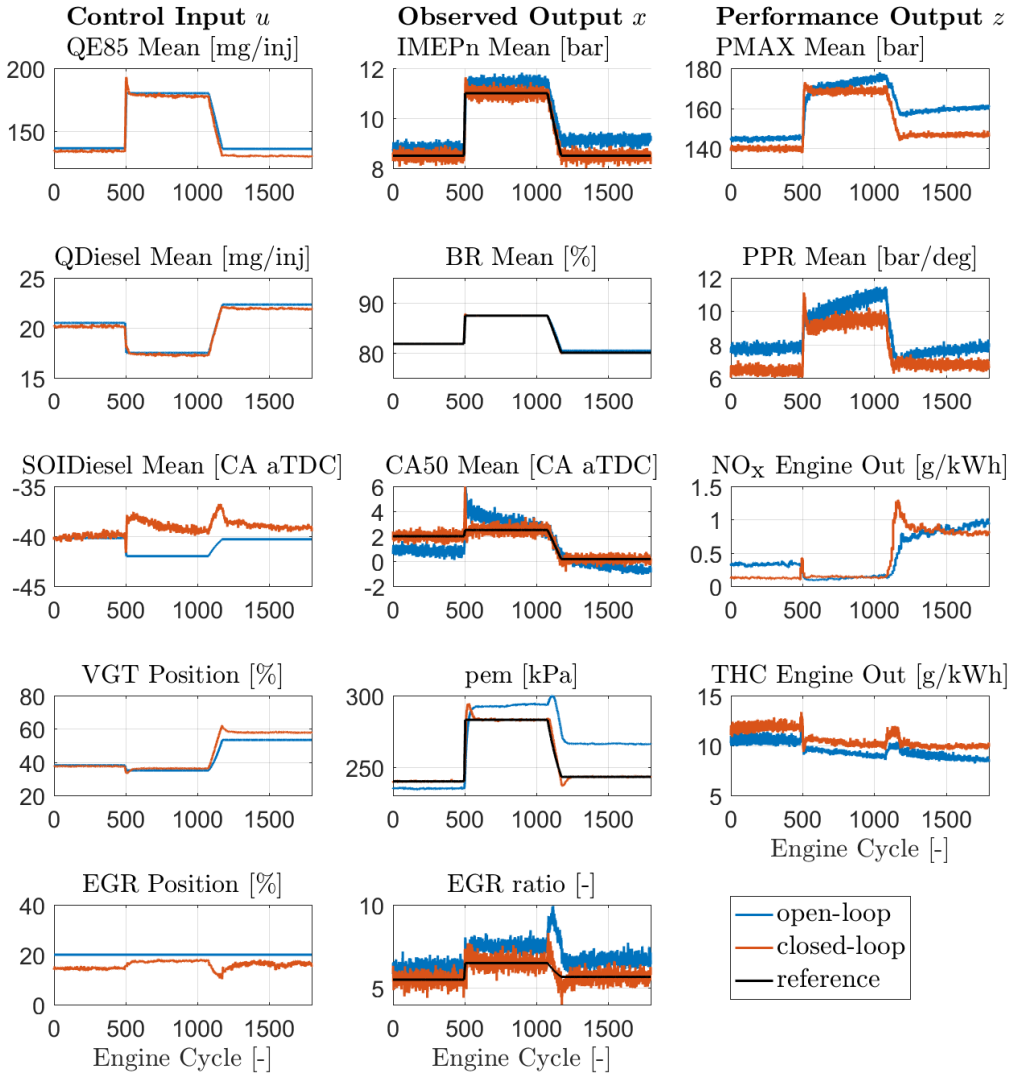

Figure 9. Transient RCCI engine performance for the proposed engine speed-load cycle: open-loop versus closed-loop results (PFI-to-SPI E85 mass flow ratio of 100%:0%). Reprinted from [19] with permission of the International Federation of Automatic Control 2020.

Table 8. Cylinder-averaged tracking results for the studied test cycle.

Performance Criteria	x_{IMEPn}	x_{BR}	x_{CA50}	x_{pem}	x_{EGR}
Average absolute error $\bar{e}_x$	0.24	0.01	0.45	1.01	0.26
Standard deviation σ_x	0.31	0.03	0.58	2.41	0.34

The results demonstrate that the closed-loop controller guarantees robust RCCI engine performance during the studied transient conditions. In addition, it minimizes the drift in z_{PMAX} and z_{PPR}, which was found in the open-loop case. This enhanced robustness gives opportunities to allow smaller safety margins. These reduced margins can be exploited to further maximize thermal efficiency or to increase RCCI load range. The later is explored in Section 5.3. For transient conditions, optimization of the reference trajectories is required to find the best trade-off between thermal efficiency and engine out emissions. It is shown that the proposed controller is able to simultaneously realize the desired air and fuel path conditions.

5.2. Disturbed Intake Manifold Temperature

To analyze the disturbance rejection capability of the RCCI engine controller, the intake manifold temperature T_{im} is gradually increased from 25 °C to 35 °C in operating point A, see Figure 10. Similar to the previous case, cylinder-averaged behavior is depicted for the open-loop as well as the closed-loop control case. For the open-loop control case, we manually determined control settings u, which keeps x around the desired r and keeps the RCCI combustion process stable. On the other hand, the closed-loop MIMO controller automatically adjusts the controller inputs to track the reference values r.

In the open-loop control case, the engine operation started at T_{im} = 27 °C with a cylinder-averaged, peak in-cylinder pressure z_{PMAX} and peak in-cylinder peak pressure rise rate z_{PPR} of 149 bar and 7.1 bar/deg CA, respectively. By gradually increasing T_{im} towards 35 °C, these values increase up to 165 bar and 11.5 bar/deg CA, respectively. Eventually, the limit for peak in-cylinder pressure rise is reached in cylinder 1 and 4, such that the engine is shut down around cycle 15,500. During the imposed T_{im} increase, we observe a significant advancement in CA50 towards TDC. This is associated with an increased end of compression temperatures. As a result, the start of combustion of the injected diesel fuel is advanced and combustion phasing is shifted correspondingly. The earlier CA50 leads to increased losses, such that cylinder-averaged IMEPn reduces from 9.7 to 9.5 bar. Moreover, due to the earlier combustion phasing, in-cylinder pressure and pressure rise levels increase. As shown in [20], engine out NO_x levels will also increase.

The closed-loop RCCI engine controller compensates for the effects of the T_{im} disturbance and controls all observed outputs x to their desired reference values r. To keep CA50 at its desired reference value of 8 degCA aTDC, diesel injection timing $u_{\text{SOI Diesel}}$ needs to be advanced significantly. At the same time, the EGR valve position is constantly adjusted between 10% opening and 30% opening. This is associated with control of x_{EGR} and p_{em} towards their reference values. This also leads to lower cylinder-averaged z_{PMAX} and z_{PPR} levels: 145 and 8.3 bar/deg CA, respectively. As a result, both outputs remain within their safety limits and safety margins are increased. It is concluded that the MIMO engine controller is able to guarantee stable and safe RCCI operation for changing external conditions that are associated with the studied varying intake manifold temperature T_{im}.

5.3. Increased RCCI Load Range

In this section, we aim to exploit the enhanced robust engine performance to increase RCCI load range. To do so, the RCCI engine is run at a constant engine speed of ω_e = 1000 rpm. For the open-loop control case, an increase in engine load τ_e is challenging.

As illustrated in Figure A3, large cylinder-to-cylinder variations in IMEPn, CA50, z_{PMAX} and z_{PPR} are observed: 2.6 bar (22%), 9.1 deg CA (149%), 39 bar (25%) and 4.9 bar/deg CA (61%), respectively, around the cylinder-averaged values. The latter compromises safe operation, since the safety limit is met. Cylinder 1 as well as cylinder 6 reach z_{PPR} = 15 bar/deg CA around cycle 5000 and 7000, respectively.

The closed-loop RCCI engine controller compensates for cylinder-to-cylinder variations and realizes the desired outputs x in all cylinders, as illustrated in Figure 11. More precisely, compared to the open-loop control case, cov(IMEPn) is reduced from 9.2% to 2.8%, whereas cov(CA50) remains small: 0.5%. Cylinder balancing indirectly leads to similar z_{PMAX} and z_{PPR} values in the six cylinders. The cylinder-to-cylinder variations are reduced by 33.6% and 11.6%, respectively, due to next-cycle combustion control.

For the closed-loop control case, the increased safety margins are used to further extend the engine's maximal load range. By manually changing the reference values r, the RCCI engine can be operated at higher loads, while still meeting the safety and noise constraints for z_{PMAX} and z_{PPR}, as defined in Table 4. In open-loop control mode, a maximum load of τ_e = 1325 Nm (BMEP = 12.9 bar) is achieved, while the closed-loop controlled RCCI engine is able to run at τ_e = 1520 Nm (BMEP = 14.8 bar), see Figure 12. This 14.7% increase in RCCI load range clearly illustrates the potential of the proposed closed-loop RCCI engine control.

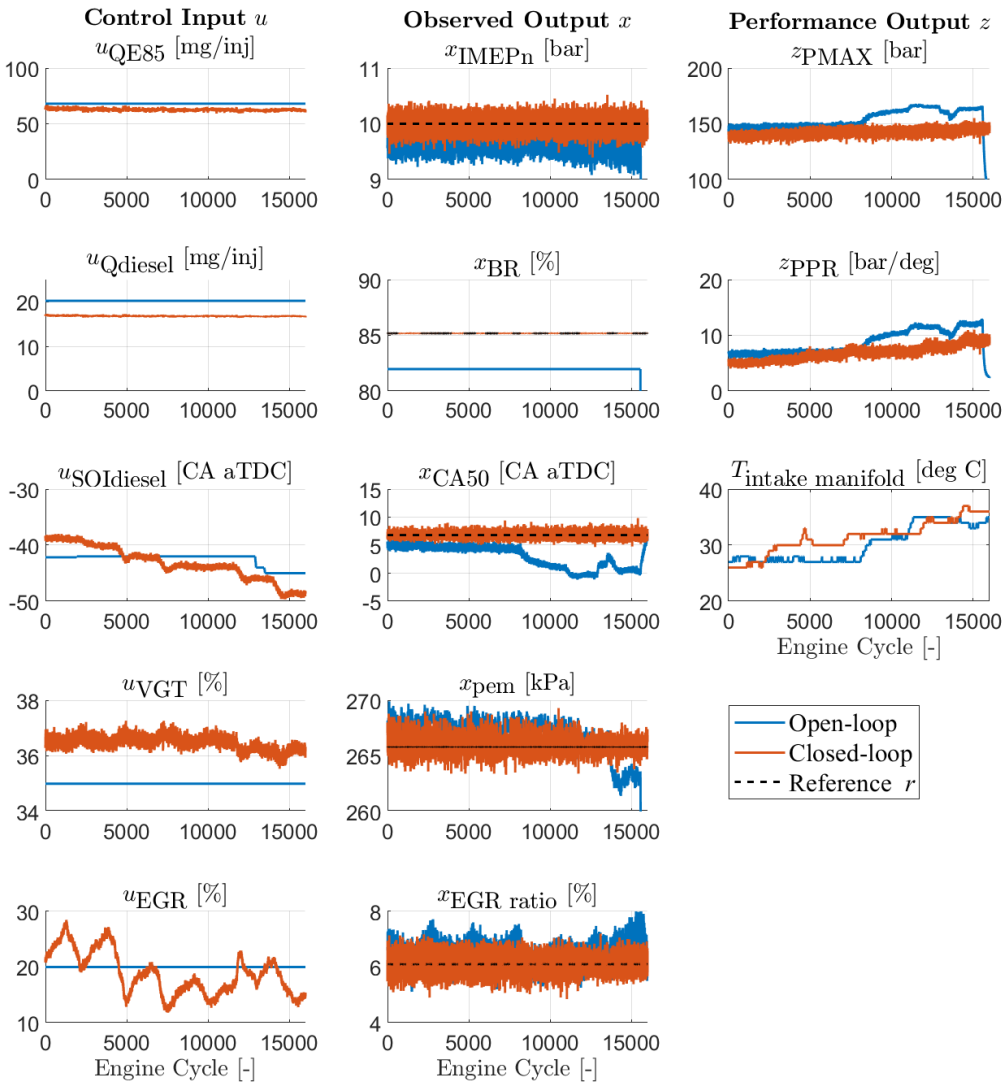

Figure 10. RCCI engine performance for disturbed intake manifold temperature T_{im}: open-loop versus closed-loop results (PFI-to-SPI E85 mass flow ratio of 50%:50%).

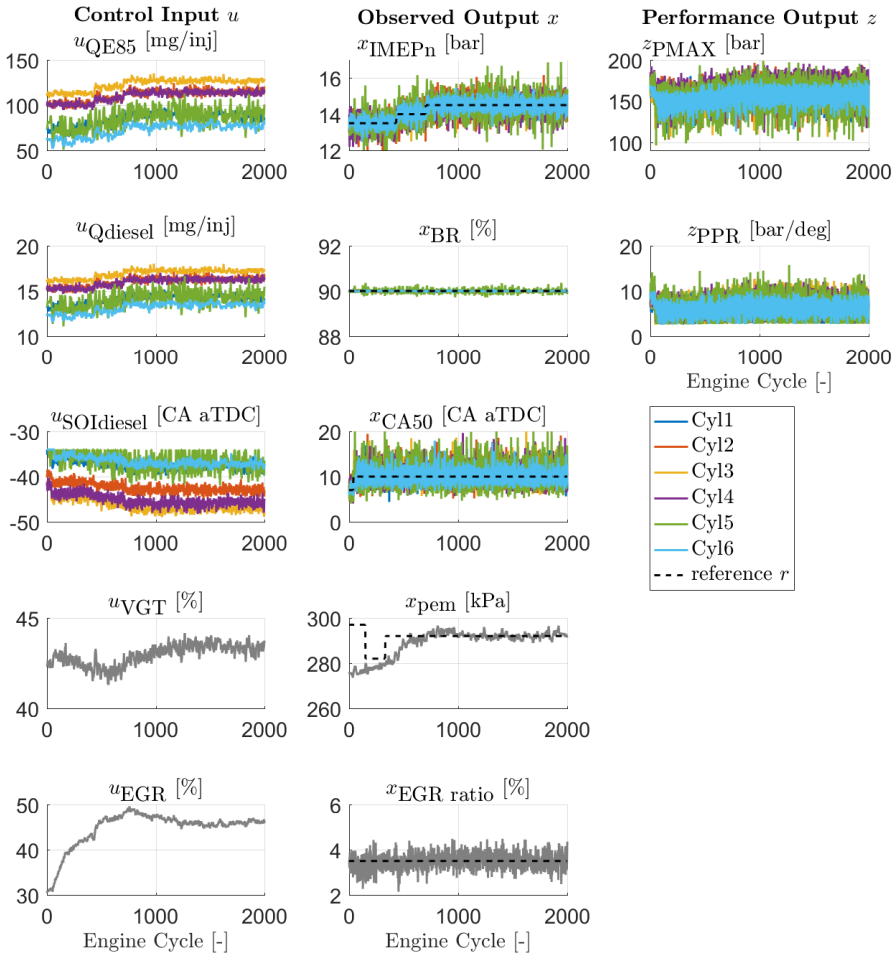

Figure 11. Engine load increase with closed-loop RCCI engine control (PFI-to-SPI E85 mass flow ratio of 50%:50%).

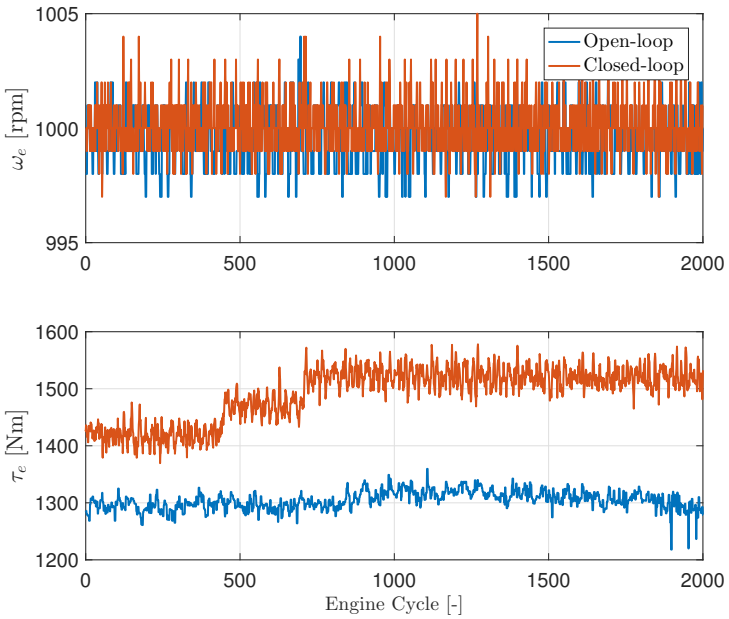

Figure 12. Demonstration of increased RCCI engine load range: open-loop versus closed-loop results (PFI-to-SPI E85 mass flow ratio of 50%:50%).

6. Conclusions

In this work, a feedforward–feedback control architecture is proposed for coordinated air–fuel path control in a multi-cylinder RCCI engine. This architecture combines static decoupling with a diagonal MIMO feedback controller and is easy to implement on a production ECU. For control design, we present a systematic, frequency response-based control design methodology, which gives clear design criteria in order to guarantee robust performance. The potential of the developed, multivariable engine controller is successfully demonstrated on a six-cylinder diesel-E85 RCCI engine. Based on the results of this study, the following conclusions are drawn:

- **Cylinder individual models of the complex RCCI combustion process can be efficiently identified following the frequency response function (FRF) method.** The resulting data-driven models also capture wall wetting phenomena and sensor and actuator dynamics and are crucial input to derive a system uncertainty model;
- **Effective input–output decoupling is realized using a static decoupling matrix.** In experiments, minimal interaction between the five control loops is observed;
- **Robust RCCI engine operation is demonstrated for the proposed closed-loop RCCI engine controller.** This controller gives good reference tracking behavior for varying engine speed and load during transients and compensates for the effect of unknown external disturbances, such as the studied intake manifold temperature variations;
- **Closed-loop engine control enables RCCI load range increase** due to enhanced safety margins. At ω_e = 1000 rpm, the maximal load range was increased by 14.7% up to BMEP = 14.8 bar.

These results are an important step in bringing RCCI engines on the road.

Future research will focus on RCCI engine performance for real-world cycles and on advanced concepts to further improve brake thermal efficiency and transient RCCI engine performance. This includes studies into the potential of electrically-assisted turbocharging [25] and DI E85 injection and of self-adaptive control strategies that on-line optimize fuel efficiency. Moreover, the use of RCCI engines in hybrid electric vehicles is of interest, see, e.g., [26].

Author Contributions: Conceptualization, J.V., F.K. and F.W.; methodology, J.V., F.K. and F.W.; software, J.V.; validation, J.V., F.K. and F.W.; formal analysis, J.V.; investigation, J.V.; writing—original draft preparation, J.V.; writing—review and editing, J.V., F.K. and F.W.; visualization, J.V.; supervision, F.K. and F.W. All authors have read and agreed to the published version of the manuscript.

Funding: This work was part of the TNO research program "Sustainable Vehicles" and was funded by the Dutch Ministry of Economic Affairs.

Institutional Review Board Statement: Not applicable.

Informed Consent Statement: Not applicable.

Data Availability Statement: Not applicable.

Acknowledgments: The authors thank their TNO colleagues Erik Doosje, Joel Groenendijk, and Kaj Mans for their invaluable support during the experiments.

Conflicts of Interest: The authors declare no conflict of interest. The funders had no role in the design of the study; in the collection, analyses, or interpretation of data; in the writing of the manuscript, or in the decision to publish the results.

Appendix A. Robust Stability Analysis for Operating Points B and C

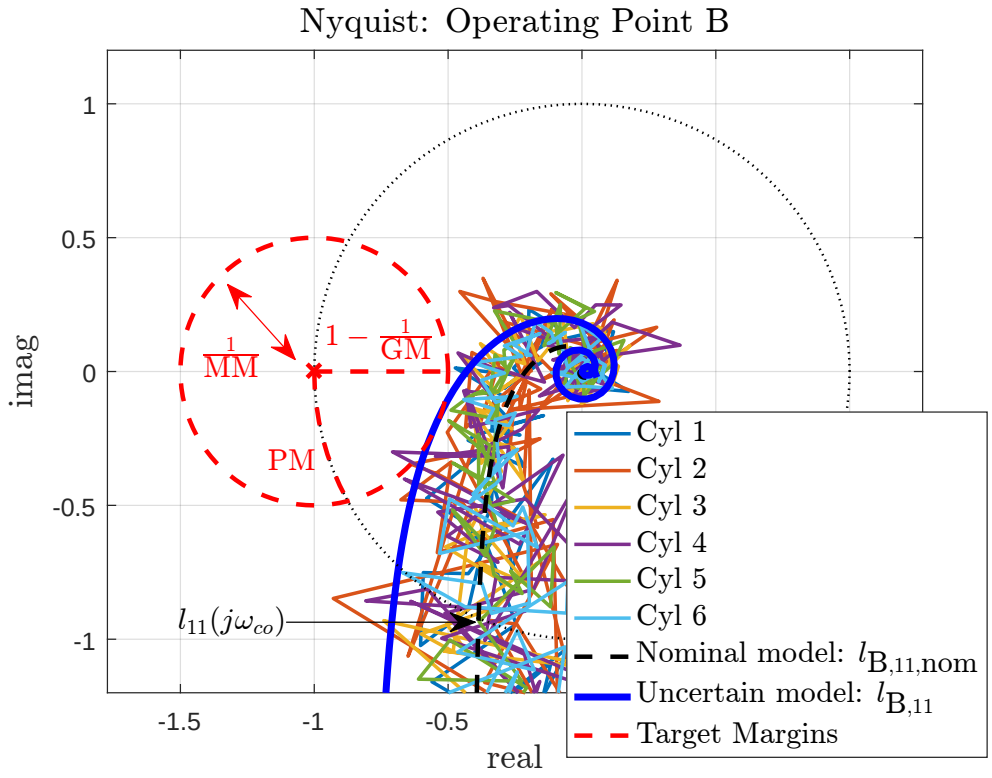

Figure A1. Nyquist plot of $l_{B,11}$ for six individual cylinders (operating point B).

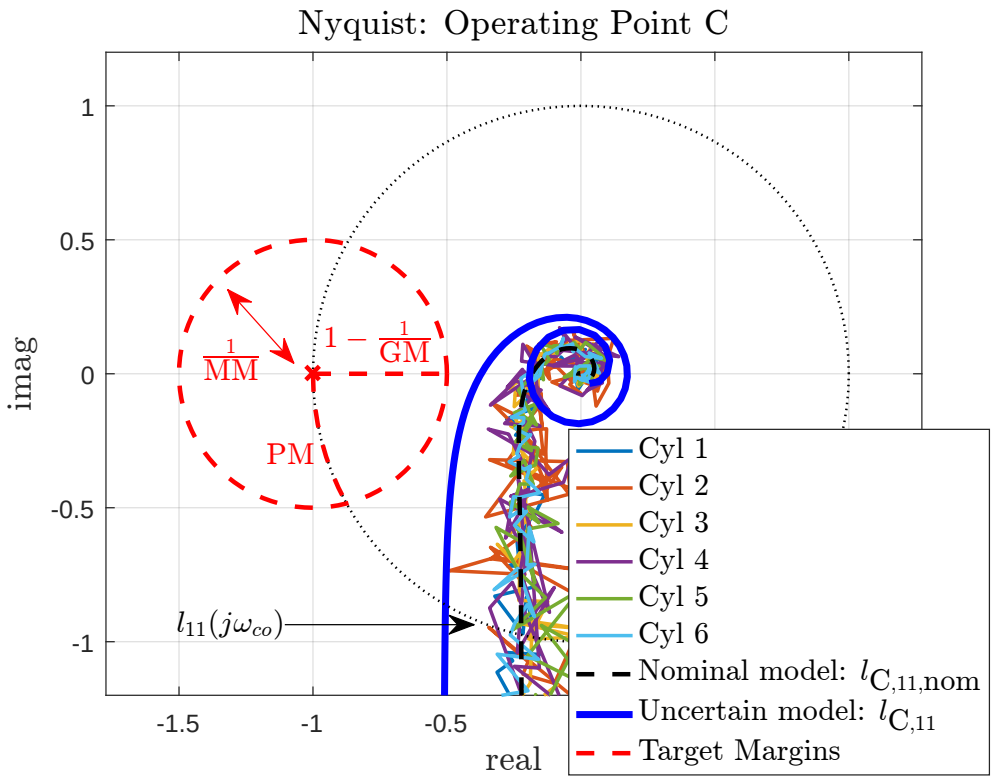

Figure A2. Nyquist plot of $l_{C,11}$ for six individual cylinders (operating point C).

Appendix B. Load Increase for Open-Loop Controlled RCCI Engine

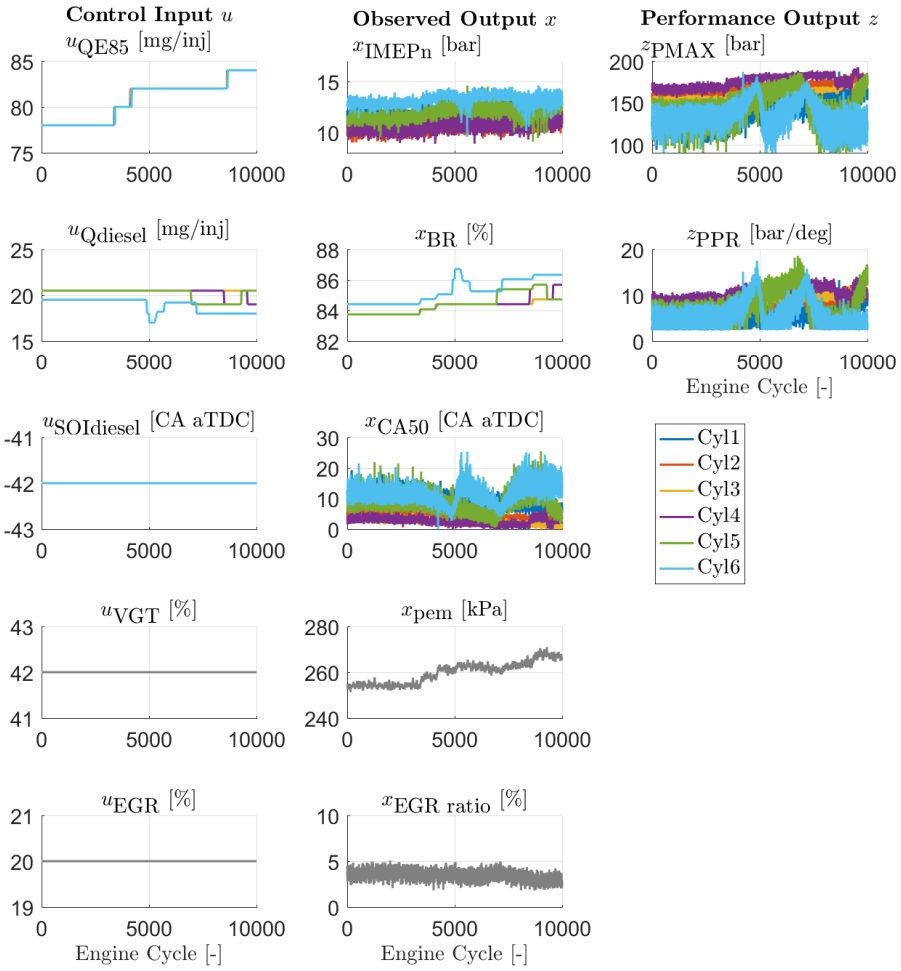

Figure A3. Engine load increase with open-loop RCCI engine control at $\omega_e = 1000$ rpm (PFI-to-SPI E85 mass flow ratio of 50%:50%). Actuator inputs are manually updated to achieve a higher load.

References

1. *A Fundamental Transport Transformation: Commission Presents Its Plan for Green, Smart and Affordable Mobility*; Press Release; European Commission: Brussels, Belgium, 2020.
2. Andersson, Ö.; Börjesson, P. The green house gas emissions of an electrified vehicle combined with renewable fuels: Life cycle assessment and policy implications. *Appl. Energy* **2021**, *189*, 116621. [CrossRef]
3. Reitz, R.D.; Duraisamy, G. Review of high efficiency and clean reactivity controlled compression ignition (RCCI) combustion in internal combustion engines. *Prog. Energy Combust. Sci.* **2015**, *46*, 12–71. [CrossRef]
4. Zheng, Z.; Xia, M.; Liu, H.; Wang, X.; Yao, M. Experimental study on combustion and emissions of dual fuel RCCI mode fueled with biodiesel/n-butanol, biodiesel/2,5-dimethylfuran and biodiesel/ethanol. *Energy* **2018**, *148*, 824–838. [CrossRef]
5. Han, J.; Somers, L.; Cracknell, R.; Joedicke, A.; W, R.; Mohan, V.R.R. Experimental investigation of ethanol/diesel dual-fuel combustion in a heavy-duty diesel engine. *Fuel* **2020**, *275*, 117867. [CrossRef]
6. Paykani, A.; Garcia, A.; Shahbakhti, M.; Rahnama, P.; Reitz, R.D. Reactivity controlled compression ignition engine: Pathways towards commercial viability. *Appl. Energy* **2021**, *282*, 116174. [CrossRef]
7. Willems, F. Is cylinder pressure-based control required to meet future HD legislation? *IFAC-Pap. Online* **2018**, *51*, 111–118. [CrossRef]
8. Olsson, J.-O.; Tunestal, P.; Johansson, B. *Closed-Loop Control of an HCCI Engine*; SAE Technical Paper 2001-01-1031; SAE: Warrendale, PA, USA, 2001.
9. Strandh, P.; Bengtsson, J.; Johansson, R.; Tunestal, P.; Johansson, B. *Cycle-to-Cycle Control of a Dual-Fuel HCCI Engine*; SAE Technical Paper 2004-01-0941; SAE: Warrendale, PA, USA, 2004.
10. Hanson, R.; Reitz, R. Transient RCCI Operation in a Light-Duty Multi-Cylinder Engine. *SAE Int. J. Engines* **2013**, *6* 1694–1705. [CrossRef]

11. Maurya, R.; Agarwal, A. *Experimental Investigation of Closed-Loop Control of HCCI Engine Using Dual Fuel Approach*; SAE Technical Paper 2013-01-1675; SAE: Warrendale, PA, USA, 2013.
12. Arora, J.; Shahbakhti, M. *Real-Time Closed-Loop Control of a Light-Duty RCCI Engine During Transient Operations*; SAE Technical Paper 2017-01-0767; SAE: Warrendale, PA, USA, 2017.
13. Raut, A.; Irdmousa, B.K.; Shahbakhti, M. Dynamic modeling and model predictive control of an RCCI engine. *Control Eng. Pract.* **2018**, *81*, 129–144. [CrossRef]
14. Guardiola, C.; Pla, B.; Bares, P.; Barbier, A. Closed-loop control of a dual-fuel engine working with different combustion modes using in-cylinder pressure feedback. *Int. J. Engine Res.* **2020**, *21* 484–496. [CrossRef]
15. Willems, F.; Kupper, F.; Ramesh, S.; Indrajuana, A.; Doosje, E. *Coordinated Air-Fuel Path Control in a Diesel-E85 RCCI Engine*; SAE Technical Paper 2019-01-1175; SAE: Warrendale, PA, USA, 2019.
16. Benajes, J.; García, A.; Monsalve-Serrano, J.; Villalta, D. Benefits of E85 versus gasoline as low reactivity fuel for an automotive diesel engine operating in reactivity controlled compression ignition combustion mode. *Energy Convers. Manag.* **2018**, *159*, 85–95. [CrossRef]
17. Splitter, D.; Hanson, R.; Kokjohn, S.; Reitz, R. *Reactivity Controlled Compression Ignition (RCCI) Heavy-Duty Engine Operation at Mid-and High-Loads with Conventional and Alternative Fuels*; SAE Technical Paper 2011-01-0363; SAE: Warrendale, PA, USA, 2011.
18. Zhang, Y.; Sagalovich, I.; Ojeda, W.D.; Ickes, A.; Wallner, T.; Wickman, D.D. Development of Dual-Fuel Low Temperature Combustion Strategy in a Multi-Cylinder Heavy-Duty Compression Ignition Engine Using Conventional and Alternative Fuels. *SAE Int. J. Engines* **2013**, *6*, 1481–1489. [CrossRef]
19. Verhaegh, J.; Kupper, F.; Willems, F. Frequency Response Based Multivariable Feedback Control Design for Transient RCCI Engine Operation. *IFAC-Pap. Online* **2020**, *53*, 14008–14015. [CrossRef]
20. Willems, R.; Willems, F.; Deen, N.; Somers, B. Heat release rate shaping for optimal gross indicated efficiency in a heavy-duty RCCI engine fueled with E85 and diesel. *Fuel* **2021**, *288*, 119656. [CrossRef]
21. Xia, L.; de Jager, B.; Donkers, M.; Willems, F. Robust constrained optimization for RCCI engines using nested penalized particle swarm. *Control Eng. Pract.* **2020**, *99*, 104411 [CrossRef]
22. Pintelon, R.; Schoukens, J. *System Identification: A Frequency Domain Approach*; IEEE Press: New York, NY, USA, 2001.
23. Skogestad, S.; Postlethwaite, I. *Multivariable Feedback Control: Analysis and Design*, 2nd ed.; Wiley: West Sussex, UK, 2015.
24. Eriksson, L.; Nielsen, L. *Modeling and Control of Engines and Drivelines*; Automotive Series, Wiley: Hoboken, NJ, USA, 2014.
25. Vlaswinkel, M.; de Jager, B.; Willems, F. Data-Based Control Structure Selection for RCCI Engines with Electrically Assisted Turbocharger. In Proceedings of the 19th European Control Conference (ECC 2021), Rotterdam, The Netherlands, 29 June–2 July 2021; pp. 491–496.
26. Poussin, O.; Gaillard, P.; García, A.; Monsalve-Serrano, J.; Martinez-Boggio, S. Dual-Fuel RCCI Diesel-Gasoline Hybrid Truck Concept to Achieve the Future Emissions Targets. In Proceedings of the 9th Aachen Colloquium China Automobile and Engine Technology, Beijing, China, 13–15 November 2019.